A R C H I V E S O F M E T A L L U R G Y A N D M A T E R I A L S
Volume 52 2007 Issue 2

H. PAUL* , **

DEFORMATION AND RECRYSTALLIZATION MECHANISMS OF LOW STACKING FAULT ENERGY METALS

MECHANIZMY ODKSZTAŁCENIA I REKRYSTALIZACJI METALI O MAŁEJ ENERGII BŁĘDU UŁOŻENIA

The microstructural evolution during deformation and light annealing of a representative low stacking fault energy metal has been characterised by detailed local SEM and TEM orientation measurements before and after annealing to partial recrystallization. High purity silver single crystals with initial (112)[11$\bar{1}$] orientation were channel-die deformed to reductions of 32% and 67%, first developing twin-matrix layers and then compact clusters of shear bands (SBs). The latter are the nucleation sites of new recrystallized grains. The as-deformed SBs exhibit large orientation spreads up to 40° with respect to the adjacent twinned areas. Most of these misorientations occur by rotations about the TD‖<110> axis with significant further rotations about <112> poles. It is suggested that slip on the two {111}<110> co-planar (CP) systems in the band can become asymmetric at large strains, leading to rotations about the <112> poles associated with local slip on one of the two CP systems. Microtexture analysis of partly recrystallized samples indicates a simple 25–40° <111> or <112> relation, frequently observed during the early stages of recrystallization between isolated nuclei and one of the two as-deformed groups of components (twins or matrix). This implies the existence of a second misorientation with respect to the other component, usually described as 50–55°<*uvw*>. During the rapid growth stage recrystallization twinning radically increases. This twinning is considered to operate after the formation of the primary nuclei.

Keywords: Shear bands, Local orientations, Texture; Recrystallization & Recovery; Silver

W pracy badano ewolucję mikrostruktury i tekstury odkształconych i częściowo zrekrystalizowanych monokrystalicznych próbek czystego srebra o orientacji wyjściowej (112)[11$\bar{1}$]. W badaniach wykorzystano zaawansowane techniki pomiaru orientacji lokalnych w TEM i SEM. Szczegółowej analizie strukturalno-teksturowej poddano dwa charakterystyczne zakresy odkształceń, tj. 32% w którym obserwowano warstwową strukturę osnowa-bliźniak nachyloną ok. 25° do KW, oraz 67% w którym to zakresie struktura osnowa-bliźniak usytuowana jest równolegle do płaszczyzny ściskania. W obydwu przypadkach na jej tle obserwowano pojawienie się makroskopowych pasm ścinania (MSB). Są one uprzywilejowanym miejscem zarodkowania nowych ziaren w procesie rekrystalizacji. W stanie zdeformowanym SB pokazują silną dezorientację przy przejściu przez obszar pasma dochodzącą do 40°, w odniesieniu do zbliźniaczonych obszarów osnowy. Osie rotacji silnie związane są z kierunkiem KP‖<110> z dobrze zarysowaną tendencją rozmywania osi w kierunku położeń <112>. W pracy wykazano związek formowania się tych dezorientacji z mechanizmami ruchu dyslokacji. Początkowy 'równowagowy' poślizg w dwu systemach współpłaszczyznowych (CP) typu {111}<011> w miarę postępu odkształcenia staje się coraz bardziej 'asymetryczny'. Prowadzi to do rotacji typu <112>, którą powiązać można z poślizgiem dyslokacji w jednym z dwu systemów CP. Analiza mikroteksturowa w stanie po częściowej rekrystalizacji pokazuje na formowanie się 25–40° (<111>–<112>) relacji dezorientacji, najczęściej obserwowaną w początkowych stadiach procesu rekrystalizacji pomiędzy izolowanym zarodkiem o jednorodnej orientacji a jednym z dwu komponentów tekstury stanu zdeformowanego (osnowa lub bliźniak). Powoduje to pojawienie się drugiego typu dezorientacji w odniesieniu do drugiej składowej tekstury stanu odkształconego, zwykle opisywanej jako 50–55°<*uvw*>. Późniejsze stadia rekrystalizacji związane są z silnym wzrostem znaczenia bliźniakowania rekrystalizującego. Pokazano, że po uformowaniu się początkowych zarodków, za pojawienie się nowych składowych tekstury odpowiedzialny jest wyłącznie mechanizm bliźniakowania rekrystalizującego.

1. Introduction

One of the major problems of recrystallization is characterizing and understanding the influence of the orientations present in the deformed state on the nucleation process, particularly in low stacking fault energy (SFE) metals. Physical intuition suggests that nuclei start from some components of the as-deformed state. There exist two major alternative models for the formation of a strong new texture, usually described as *'orientation nu-*

* INSTITUTE OF METALLURGY AND MATERIALS SCIENCE, POLISH ACADEMY OF SCIENCES, 30-059 KRAKÓW, 25 REYMONTA STR., POLAND
** UNIVERSITY OF ZIELONA GÓRA, MECHANICAL DEPARTMENT, 65-246 ZIELONA GÓRA, 50 PODGÓRNA STR., POLAND

cleation' (ON) or *'oriented growth'* (OG). The ON model is the hypothesis that grains, with an orientation that dominates the fully recrystallized texture, nucleate more frequently than do grains of all other orientations. On the contrary, the OG hypothesis assumes that grains with a particular orientation attain sizes significantly larger than the average diameter of the recrystallized grains. The basis for such an approach have been the observations of high mobilities of recrystallization fronts of certain misorientations. The ON and OG models describe the phenomenon of the recrystallization texture quantitatively, but totally neglect determination of the mechanisms giving rise to the effects.

Previous work [1–12] has shown that during cold rolling, or plane strain compression, {112}<111>-oriented crystals or grains of low stacking fault energy (SFE) face centred cubic (fcc) metals always undergo twinning and shear banding processes. In grains containing narrow, freshly formed shear bands (SBs), the twin-matrix (T-M) plates undergo rotations towards the shear plane [3–8]. Thus in crystals of Cu-2%Al [8–11] or Cu deformed at 77K [5, 12], this rotation occurs mainly around <110>||TD leading to the formation of two main groups of components near G{110}<001> (or Goss) for the twins and G^T{114}<221> for the matrix. After further plastic strain the near Goss-oriented areas undergo local <112> rotations, ultimately leading to the formation of texture components near S{123}<634> or Brass{011}<112> (B) [12].

The recrystallization mechanisms in deformed low SFE fcc polycrystals are often difficult to characterize because of the complexity of the deformation microstructures; the latter usually result from a combination of dislocation glide and fine mechanical twinning into T-M layers and then, at higher strains, shear banding at different scales. Pure silver with a SFE = 22mJ/m^2 [13] is typical of many such low SFE fcc metals and alloys. The complex microstructures of deformed low SFE polycrystalline metals and alloys have limited progress in this area, but can be simplified by using a model material in the form of oriented single crystals [14–19]. Shear bands represent local regions of high stored energy compared to the surroundings and therefore constitute highly potent sites for recrystallization nucleation. However, how the shear bands modify the global texture is still an open question.

The main goal of the present work is to understand the formation mechanism of new grain orientations at the early stages of recrystallization in low SFE metals, paying particular attention to the specific microtexture components of SBs. Plane strain compressed Ag single crystals of the (112)[11$\bar{1}$] (C or copper) orientation are particularly interesting, since they form SBs which penetrate the whole thickness of the sample [11]. They lie along a plane parallel to the transverse direction (TD) so that longitudinal sections give all the required information. The SBs are usually grouped into clusters, which make up macroscopically visible shear bands (MSBs). The annealing conditions can be designed to facilitate recrystallization inside SB-saturated structures, thus eliminating any nucleation events associated with twin boundaries lying outside the bands and hence facilitating the crystallographic analysis of the deformed and recrystallized states. The controversies over the nature of the mechanisms responsible for the formation of new nuclei and the introduction of new research methods to resolve these mechanisms motivated this work. This is especially important for low SFE metals.

Throughout this study the local crystallography is examined in detail by scanning (SEM) and transmission (TEM) electron microscopy using electron backscattered diffraction (EBSD) and convergent beam electron diffraction (CBED), respectively.

2. Experimental procedures

High purity Ag crystals with C(112)[11$\bar{1}$] initial orientation, obtained by the Bridgman method, were sectioned in the form of 10×10×10mm cubes. The Teflon^{TM} lubricated samples were deformed up to 90% at room temperature and a nominal strain rate of $10^{-4}s^{-1}$ in a channel-die, using multi-stage tests to form SBs and their compact clusters, macroscopic shear bands (MSBs). Two strain levels were analysed in detail corresponding to thickness reductions of 32% and 67%. Some of the bulk deformed samples were sectioned perpendicular to TD, using a wire saw, to ~2 mm thick slices to provide samples for the annealing treatments. Annealing was carried out in an air furnace for 30s at temperatures of 265°C and 300°C before quenching into water.

The detailed microtexture evolutions during recrystallization nucleation and growth were analysed by modern techniques using TEM and SEM. For nanoscale analyses the local orientations were characterized by TEM using a 200 kV PHILIPS CM200 with semi-automated Kikuchi line based analysis. The thin TEM foils were prepared by a twin-jet technique in standard methanol – nitric acid solution. TEM methods were used to examine the dislocation substructure in relation to changes in microtexture in the as-deformed and partly recrystallized samples. Microstructure observations and systematic local orientation measurements were also examined in a JEOL 6400 and 6500F SEM, using backscattered electrons at 20 kV to reveal crystallographic contrast. Both SEMs were equipped with facilitates for EBSD. Microscope control, pattern acquisition and solution were car-

ried out with the HKL Channel 5 system. In all cases a step size within the range of 0.2–1 μm was applied. For more global (sample scale) microstructure observations optical microscopy was used on mechanically and chemically polished samples.

Local orientation data, obtained by TEM and SEM on the ND-ED plane (where: ND – normal direction, ED – extension/rolling direction) were transformed to the standard ED-TD reference system and presented in the form of {111} pole figures and/or distributions of the misorientation axes.

3. Results

3.1. Deformed state. The shear band structures and textures

Figure 1 shows a stereographic projection of the characteristic orientations, resulting from the systematic changes of the initial crystal orientation, produced by plane strain compression (PSC) involving glide and twinning. All these orientations are developed by TD rotations, i.e. about the <110> direction. Slip geometry of the C-oriented fcc single crystal with marked co-planar (CP) and co-directional (CD) slip systems is shown in Fig. 1b. On the longitudinal section, the slip plane traces and ED form the angles of 19.5° and 35.3° for CP and CD, respectively.

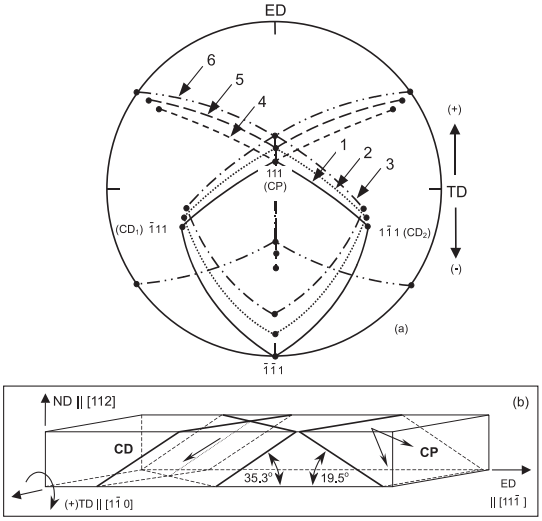

Fig. 1. (a) Stereographic projection showing the orientation changes during plane strain compression of an initial C(112)[11$\bar{1}$] oriented crystal as a result of (+)TD//[1$\bar{1}$0] rotation and twinning. (b) Corresponding schematic presentation of the {111} slip planes in the sample. The following characteristic orientations are shown: 1-C(112)[11$\bar{1}$], 2-D(4 4 11)[11 11 $\bar{8}$], 3-(114)[22$\bar{1}$], 4-(552)[$\bar{1}\bar{1}$5], 5-D^{Twin}(26 26 5)[$\bar{5}$ $\bar{5}$ 52], 6-G(110)[001]

The essential part of the experimental stress-strain curve, $\sigma = f(\varepsilon)$, as presented in Fig. 2a, clearly indicates a non-monotonic increase in stress as a function of strain. Stress and strain were calculated by $\sigma = F/A$ and $\varepsilon = ln(h_o/h)$, where F, A, h_o and h are the current compression load, sample compression surface, and initial and current specimen thickness, respectively. All the samples, after an initial reduction of about 10-15%, exhibit repeated stress serrations typical of deformation twinning. The periodic stress relaxations, with stress variations of about 10 MPa, began after an abrupt stress drop. Over this strain range, the periodic, high frequency stress relaxation is associated with the propagation of deformation twins through the sample thickness. At deformations above about 0.3 the stress oscillations die out and macroscopic compact clusters of SBs are formed.

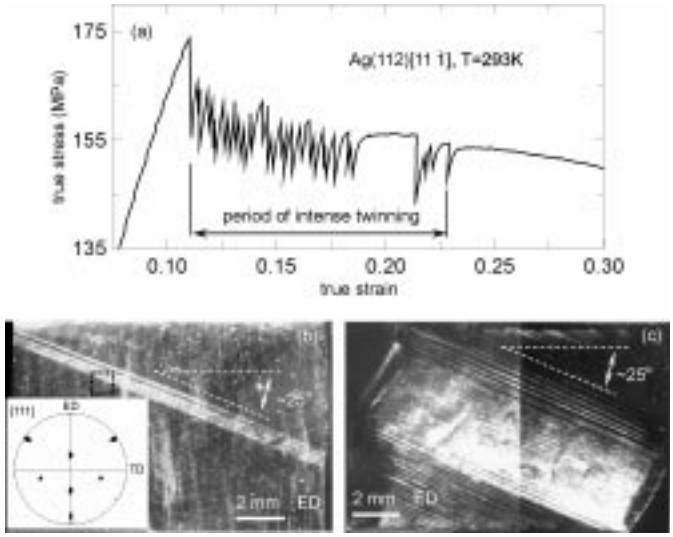

Fig. 2. (a) True stress-strain curve of silver single crystals within the range of intense mechanical twinning. The successive stages of twinning at the sample scale. Silver single crystals compressed: (b) 11% and (c) 19%. Optical microscopy on ND-ED plane

As in most low SFE fcc metals, the initial microstructure of a deformed Ag single crystal is composed of the near-initial matrix and the twin related areas. Figure 2b illustrate successive stages of the formation of twin areas from 11 to 19% reductions. The concentration of twins in a broad band (Figs. 2a and b), initially inclined at about 25-27° to ED and clearly observed in the longitudinal plane at 11% and 19% strains, indicates that the twinning process starts on the (111) plane from orientations which have deviated from the initial C(112)[11$\bar{1}$] orientation towards the so-called Dillamore component, i.e. D(4 4 11)[11 11 $\bar{8}$] (twins lie on planes inclined about 27.4° to the compression plane). This is confirmed by the {111} pole figure (see detail in Fig. 2b) which shows high intensity <111> poles of the matrix at the D position, 8°(+) TD rotated from the initial position, and also the large twin-induced rotations to D^{T}(26 26 5)[$\bar{5}$ $\bar{5}$ 52]. This result, in agreement with Wagner et al. [20] and Paul et al. [9–12], confirms that in

C-oriented fcc single crystals the twinning process starts after the lattice rotation towards the D-orientation. Note also that, as a result of shear along the twinning planes, characteristic sample shape changes are observed on the free surface (Fig. 2c).

3.1.1. MSB formation at the sample scale

The microstructure of fine T-M layers is very anisotropic and resistant to homogenous deformation by slip across the twin boundaries. This severely restricts the possibilities of homogeneously accommodating additional strain. Furthermore, the contact of the sheared parts of the crystal with the compression tools induces then a global rotation of the twinning planes towards the compression plane, clearly visible at 32% reduction. The beginning of this movement coincides with the initial stage of strain localization in the form of MSBs (Fig. 3a) and further shear along the SB direction (see Figs. 3b and c) and propagation of the SB across the sample. The bands of localized strain, separated by areas of relatively weakly deformed twinned matrix, exhibit a strong tendency to form groups of compact bundles.

Fig. 3. The successive stages of macroscopic shear band formation at the sample scale. Silver single crystals compressed: (a) 32%, (b) 43% and (c) 67%. Optical microscopy on ND-ED plane

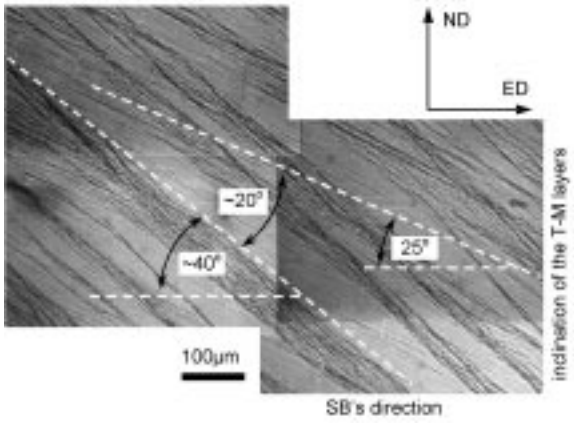

Fig. 4. A detail showing macroscopic shear band formation against a background of twin-matrix layers in a sample compressed 43%. Optical microscopy on longitudinal section

Higher magnification observations (Fig. 4) in the ND-ED plane of an MSB area of a sample deformed 43% shows the MSBs to be composed of clusters of single SBs and inclined at 40-42° to ED. This also reveals that MSBs are formed against a background of strongly twinned matrix, containing only needles of primary matrix. For the situation shown in Fig. 4 the T-M layers are inclined at ~ 25° to ED, and form an angle of about 20° with respect to the SB. The bands are rather irregularly spaced, and tend to form compact clusters. Clearly the band directions do not coincide with the traces of the (111) twinning plane, nor with the other {111} planes within the neighbouring areas, as often noted previously, e.g. [2, 3]. This can lead to premature conclusions about the non-crystallographic character of these bands.

3.1.2. Local lattice rotation observed at the mezo-scale. SEM/EBSD orientation mapping

The microstructures of C-oriented Ag single crystals deformed to high strains conserve relatively thick needles of primary matrix as well as new twins. Consequently, two well- defined groups of orientation components (matrix and twins) make up the as-deformed texture.

For medium deformations (30–40%), the T-M layers within the MSB show a strong tendency to rotate nearly parallel to the shear plane. Figure 5a shows the microtexture components of an area occupied by a primary set of MSB (see Fig. 3a) in a sample deformed 32%. Two groups of orientations are identified on the {111} pole figure of this area: $G(110)[001]^T$ and $G^T(114)[22\bar{1}]^M$ with further (+/-)10° TD scattering. In this case the orientations resulting from (+)10° TD rotations are described by $(118)[44\bar{1}]^M$ and $(17\ 17\ \bar{4})[2\ 2\ 17]^T$ components. At these early stages of SB formation large areas (of about 1mm) undergo rotation.

At a deformation of 67% the MSBs have grown and occupy a significant volume of the crystal (see Fig. 3c). Systematic local orientation measurements from the area marked in Fig. 3c are presented in Fig. 5b, where the

microtextural effects resulting from the positions of the T-M layers outside the SB and twinned matrix inside SB are shown. In this case the needles of primary matrix outside the band are nearly parallel to the compression plane, whereas the SBs are inclined at about 25°–35° to ED. The spread of the <111> poles corresponds to twin and matrix positions. At the limit they can be described by two twin-related groups, lying near $(110)[001]^{T}$ + $(114)[22\bar{1}]^{M}$ positions (for (+)TD scattering) and a second pair $(775)[5\ 5\ \bar{1}4]^{T}$ and $(17\ 17\ 23)[\bar{2}3\ \bar{2}3\ 34]^{M}$ (for (−)TD scattering). The observed scattering of the <111> poles is significantly broader than that observed at lower deformations, but the orientations at the maximum (+)TD deviation are nearly the same. This broad scattering results from the inclinations of the T-M layers outside the band which, in this case, are situated nearly parallel to the compression plane.

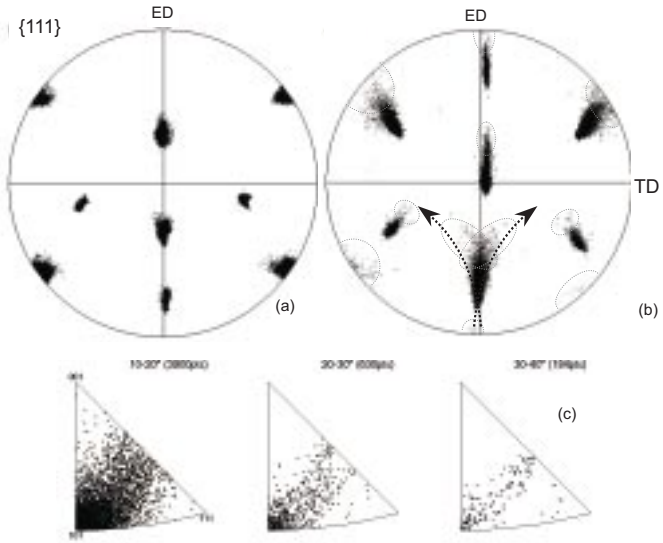

Fig. 5. {111} pole figures showing the microtexture components inside an MSB in samples deformed (a) 32% and (b) 67%. (c) Essential part of the misorientation axes distribution for relations between neighboring pixels of an OIM (67% thickness reduction). Local orientation measurements by SEM/EBSD. Step size of 200 nm

The distributions of the misorientation axes for the samples deformed 67% and for areas containing primary sets of MSB are given in Fig. 5c. The misorientation axes are grouped into two populations. One is due to the deformation twins and the formation of 60°<111> type misorientations. The other lies near the <110> direction within a broader range of angles up to 40° and rather unexpectedly exhibits a clear scattering of the misorientation axes towards <112>.

3.1.3. Nanoscale lattice rotation within SB: TEM local orientation measurements

The very first plastic instability, i.e. the initial distortion of the T-M lamellae within narrow areas by which shear banding begins, is similar to that observed at the optical microscopy and SEM scales. The thickness reductions of 32% and 67% gave rise to two quite distinct deformation microstructures which could be expected to influence recrystallization: the lower strain corresponded to the early stages of MSB formation when the twinning planes outside the MSB family were inclined at 25° to the compression plane (Fig. 6a), whereas after the higher strain the twinning planes outside the MSB family lay nearly parallel to compression plane (Fig. 6b). The latter situation was typically observed at large strains in all low-SFE fcc metals. The initial stages of strain localization coincide with the appearance of lattice deflections inside restricted areas [2, 9–12]. The sense of this deflection can be described by (+)TD scattering of the T-M layers, with an increasing inclination of the twinning planes with respect to ED.

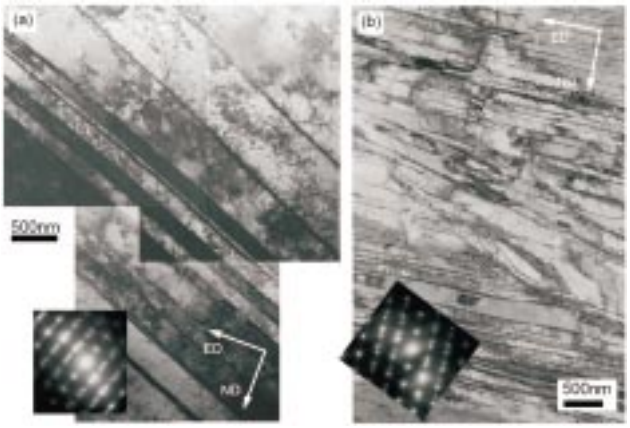

Fig. 6. TEM microstructure showing the twin-matrix layer structure in a sample deformed: (a) 32% and (b) 67%. Selected area diffractions indicate orientations of the twinned matrix

Figure 7 shows the TEM microstructure of a sample compressed 43%, representing an early stage of brass-type SB formation (along a line inclined about 40° to ED). The fine structure of T-M lamellae, with twinning planes inclined about 20-22° to ED is typical of low SFE metals at moderate strains. Localized shear is associated with ~20° rotation of the material inside the SB, together with a relative displacement of the twinning planes outside the band. The sense of this rotation is such as to increase the inclination of the twinning planes with respect to ED, i.e. it is opposite to that of the general T-M lamellae. Measurements of local orientations within the bands by using TEM point to the occurrence of (+)TD scattering of the <111> poles lying near Goss{110}<001> position, deviated by about 20° (+)TD from the twin position outside the band (Figs. 7b and c); this corresponds to the transition from orientations very close to $(221)[\bar{1}\bar{1}4]^{T}$ towards positions close to (110)[011]. The absence of matrix orientations within

the bands has been described in detail in a previous work [12] and will not be discussed here.

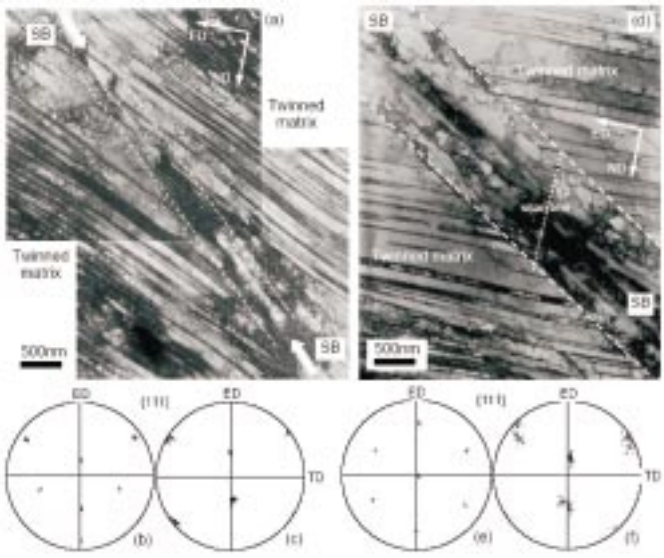

Fig. 7. (a) TEM microstructure showing the onset of instability of the twin-matrix layer structure in a sample deformed 43% and corresponding 111 pole figures showing microtexture for: (b) twinned matrix outside the band and (c) within SB. (d) TEM microstructure showing well-developed shear band in a sample deformed 67% and corresponding 111 pole figures showing microtexture for: (e) twinned matrix outside the band and (f) within SB. TEM local orientation measurements

Well-developed SBs (sample deformed 67%) were exemplified by the broad SB of Fig. 7d, formed against a background of T-M layers. At the SB boundary this T-M layered structure usually changes its inclination, varying from 20° to about 30° to ED, indicating a gradual incorporation of the structure outside the band into the band[1)]. The internal structure of SB is composed of very fine sub-grains highly elongated along shear direction. 1 μm thick SBs, inclined at 35–40° to ED, are typically formed at moderate deformations. The microtextures of T-M layers and within the band are presented in Figs. 7e and f, respectively. The orientation of the T-M layers can be described by a position close to {111}<112>^{T,M} (for the twins and for the matrix). The shear bands orientations are grouped again near Goss{110}<001> position and again show the absence of the matrix orientation (Fig. 7f). The maximum density of the band orientations (near G{110}<001>) results from the 15-25° (+)TD rotations of areas associated with the twins outside the SB. However, the interpretation of the real lattice re-orientation within SB is more complex than this simple TD rotation.

TEM orientation line scans within the SB of Fig. 8 reveal large orientation spreads of up to 35-40°; most of these misorientations occur about the TD‖ <110> axis, but at these high strains there are significant further rotations about one of the two <112> poles close to TD. This is the basis of the suggestion by Paul et al. [12, 21, 22] that slip on the two co-planar (CP) slip systems in the band becomes progressively asymmetric, i.e. the rotation about one of the two <112> poles corresponds to local slip on one of the two {111}<110>-type slip systems. The progressive rotation inside the bands which is responsible for lattice bending and the general texture transformation, describes the lattice rotation from twinned matrix to the band positions. In this way the mechanism of advanced band development is crystallographic and *connected with a single slip operation*.

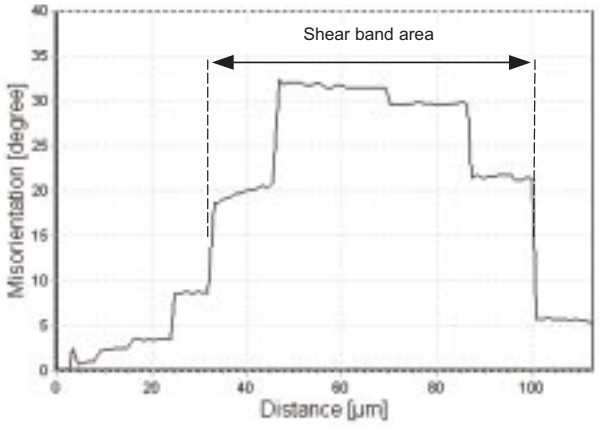

Fig. 8. (a) Misorientation profile with respect to the first measured point within twin lamellae, along the line scan across the SB presented in Fig.7(d). TEM local orientation measurements

3.2. Recrystallized state

3.2.1. The global microtexture development during the early stages of recrystallization

Fig. 9a and b show examples of a partly recrystallized microstructure observed at optical microscopy scale and obtained by SEM/EBSD measurements, respectively. Both microstructures show that new grains are formed only in the MSB areas.

At 50% reduction the lamellar structure of fine, alternating T-M layers is broken up by compact SB clusters inclined at 35-40° to ED (Fig. 9a) which constitute the preferred nucleation sites of new, recrystallized grains. Σ3(60° <111>) twin boundaries, visible as bold, black lines on the orientation map, obtained after 67% reduction (Fig. 9b), are developed within several recrystallized areas. There are, however, no recrystallized areas which are twin related to the deformed state, suggesting that recrystallization twinning (RT) is a secondary mechanism, occurring after the formation of primary nuclei

[1)] This is clearly visible at the early stages of SB formation as a result of reduced stability within narrow zones [8].

of uniform orientation. The {111} pole figure containing only the as-deformed orientations is given in Fig. 9c and shows the matrix and twin orientations plus their spread due to SB formation. After short annealing the recrystallized grain orientations are represented by the {111} pole figures of Fig. 9d; they show significant differences with respect to the as-deformed microtexture. However, there is a tendency for certain orientations (shaded in the figure), situated at the limit of the deformation microtexture range, to participate in the nucleation process. In the as-deformed state, SB orientations are only weakly visible on the 'global' deformation texture and are located at the limit of their spread (at the (+)TD rotated boundary). At the early stages of primary recrystallization, these <111> poles become sharper. As recrystallization proceeds and α(<111>–<112>) rotations are developed in selected areas of the band, the intensity of the <111> pole of the most active {111} planes during deformation systematically increases. This mechanism, as will be demonstrated below, is in fact due to the retention of particular <111> poles of the deformed state in new positions, which correspond to the recrystallized grain.

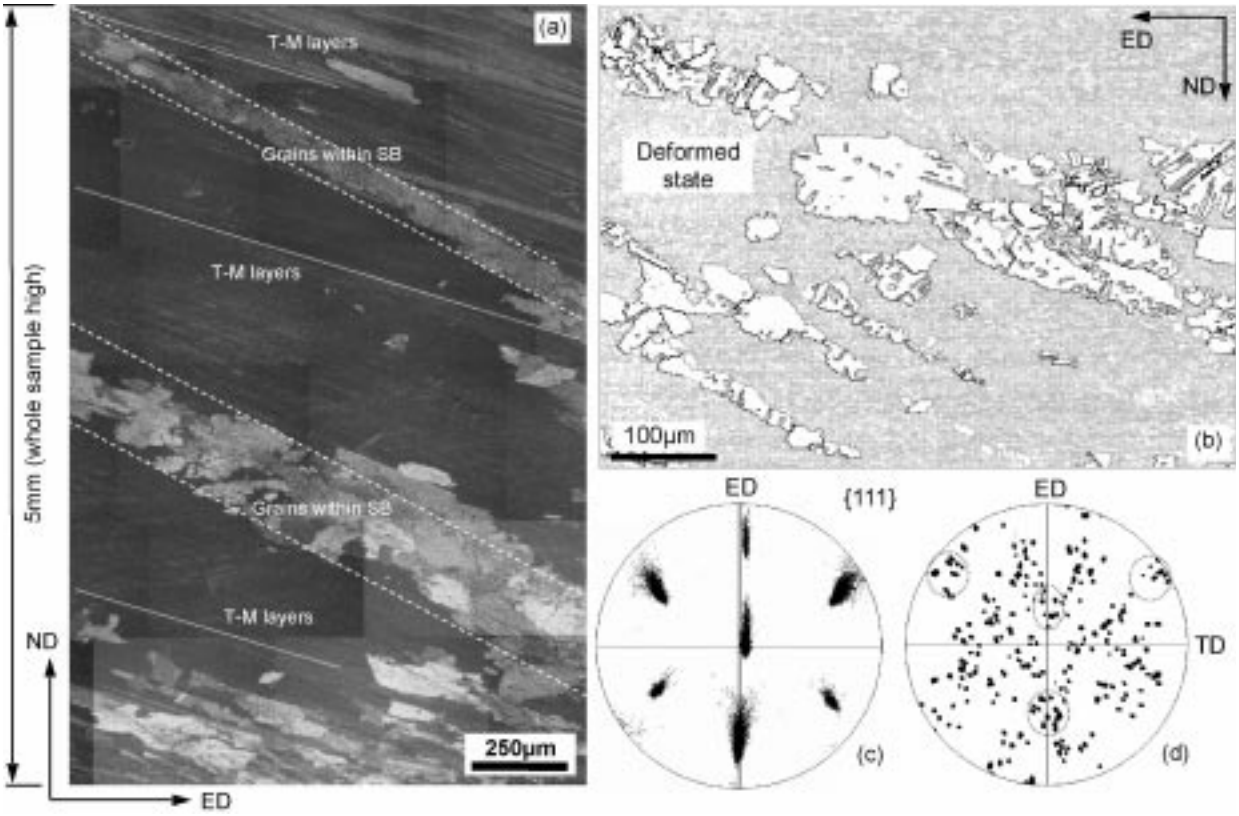

Fig. 9. Partial recrystallization in silver. (a) Microstructure observed in optical microscopy scale on longitudinal section of a sample deformed 50%. (b) Grain boundary map for a sample deformed 67% and annealed 30s at 265°C. (c) and (d) {111} pole figures containing only as-deformed and recrystallized areas, respectively. SEM/EBSD measurements with step scan 1 μm. Shaded areas represent as-deformed SB orientations

3.2.2. The early stages of recrystallization (TEM analysis)

After short annealing strong recovery occurs before and during recrystallization and leads to a drastic decrease of the dislocation density within the internal SB substructures. Figure 10 is a TEM image of the longitudinal {110} section, revealing a well-developed dislocation network tending to a cell substructure. The dislocation density in the cell walls decreases and isolated dislocations and narrow dislocations dipoles have annealed out from the cell interior.

The nucleation and the subsequent recrystallization growth process occur in the same way for all deformations (up to 1.5). A nucleus is considered to be a region of uniform orientation, typically <1 μm diameter, developed usually within a substructure of heavily dislocated and elongated cells (of width ~0.2–0.5 μm). In the present study only a limited number of primary nucleus orientations were detected; all were associated with

α(<111>–<112>)-type rotations around selected axes in accordance with a previous work [23].

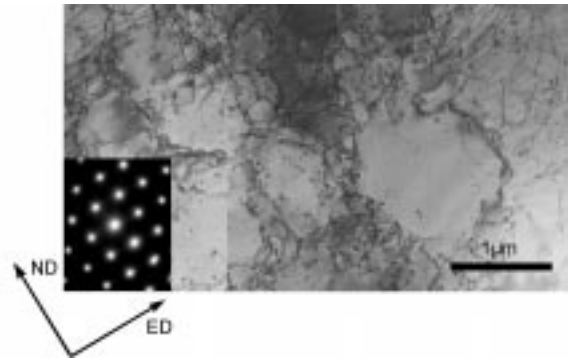

Fig. 10. TEM bright field images showing strongly recovered dislocation structure formed at the early stages of recrystallization. Observations carried out on the longitudinal section of a crystal deformed 67% and annealed 265°C for 30s

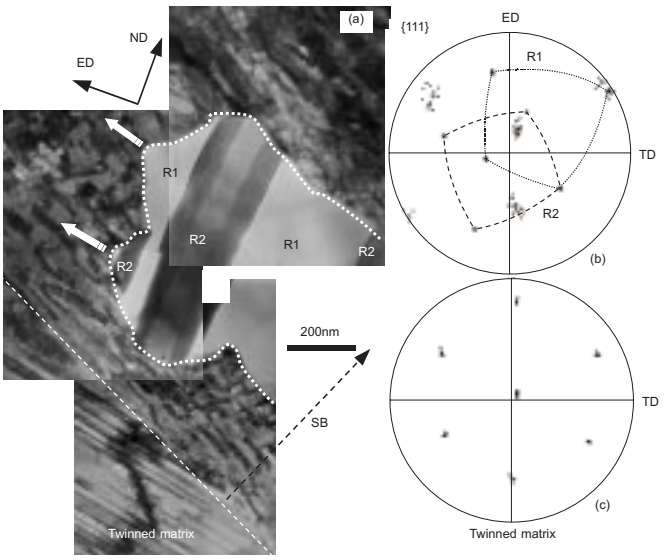

Fig. 11. Nucleation and growth of a new grain in Ag crystal deformed 67% and annealed 30s at 265°C. (a) TEM bright field image and corresponding {111} pole figure containing orientations: (b) of the nuclei (R1 and R2) and as-deformed area orientations within shear band, (c) twinned matrix outside the SB. TEM local orientation measurements

A more advanced stage of recrystallization is illustrated in Fig. 11a, for the case of a large grain growing along a shear band. The recrystallization front is very irregular, indicating different local growth rates due to local variations in misorientation as a consequence of the orientation spread in the as-deformed areas (Fig. 11b). The orientations of the twinned matrix are presented in Fig. 11c. A detailed TEM analysis of the orientation relations along the recrystallization front indicates that the highest local growth rates (where the recrystallized grain is pulled forward) occur where there are pronounced lattice disturbances, around <111> or <112> axes, of the deformed structure within the band [23]. Then the growing grain tends to consume these highly localized regions, resulting in an elongated shape along the band direction. The shape of the recrystallization front results from its strong tendency to grow preferentially along the dislocation-rich layers within the bands. The segment of the grain boundary pulled forward (indicated by white arrows) is considered to be the most mobile part and its orientation relation, between the recrystallized grain and the adjacent deformed structure (described again by the position of twins within the band), can be described as 30-35°(<655>–<211>). In this case the migrating boundary of the growing grain is developed inside the structure of the shear band.

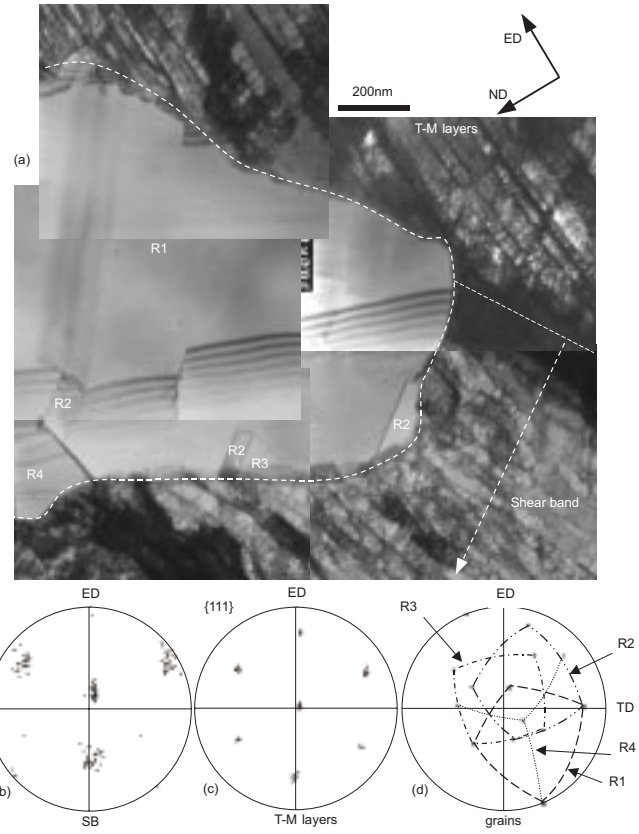

Fig. 12. (a) TEM microstructure showing growth of a new grain in Ag crystal deformed 67% and annealed 30s at 265°C. (b)-(d) Corresponding {111} pole figures for particular areas: (b) as-deformed orientations identified within SB, (c) as-deformed orientations identified within SB and (d) orientations of the recrystallized grains

Another case of the recrystallized phase growth is observed in Fig. 12, where the new grain completely filled the structure of the SB. In this case the growth process occurring along the SB/(T-M) boundary implicated the occurrence of a quite different type of misorientation relations, i.e. between the new grain and the structure of T-M layers. The existence of the layered structure within the deformed state also means that a particular orientation relationship with respect to one component of the deformation microtexture leads to another misorientation with respect to the other component. In some

cases the recrystallized grain can grow into this layered structure; however the mechanism of this process is not quite clear. The orientations identified within recrystallized phase show only twin relations, i.e. particular parts of the recrystallized grain (R1-R2, R1-R3 and R1-R4) are twin related.

3.2.3. The crystallography of the recrystallization growth stages (EBSD analysis)

In this section the different stages of recrystallization nucleation and growth are analysed by EBSD orientation maps as a complement to the TEM work on nucleation. They can be described as: (i) the formation of single isolated nuclei of uniform orientation from twins, or more rarely from the matrix, (ii) the early stages of recrystallization growth and the first recrystallization twins and (iii) the formation of chains of different nuclei by recrystallization twinning. All orientation maps are presented as grain boundary maps. Some of the above cases will be now analysed in greater detail.

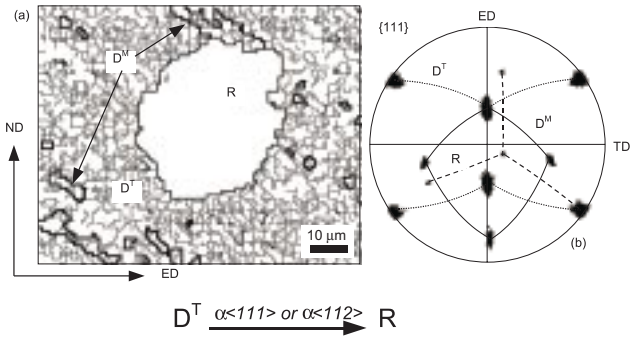

Fig. 13. Nucleation of a single grain of uniform orientation. (a) part of the 'grain boundary' map. (b) {111} pole figure showing the recrystallized grain and the nearest as-deformed neighbourhood orientations. Sample deformed 32%. SEM/EBSD measurements

The single grains of uniform orientation. Figure 13a is a part of orientation map ('grain boundary' map) and illustrates a single isolated nucleus of uniform orientation, observed after 32% strain, which tends to grow within the SB. At this deformation degree the MSB deformation structure is composed of deformation twins and primary matrix, where the latter appears in the form of relatively thick needles. The twin boundaries identified within the deformed state (bold, black lines) are aligned along the band direction, but no twins are observed within the recrystallized grain nuclei in this case. The {111} pole figure of Fig. 13b shows the orientations of the grain and the adjacent as-deformed areas. A detailed analysis of all the misorientations in different directions clearly shows that the ~25°<111> type relation occurs where there is a tendency to grow into the areas of D^T orientations.

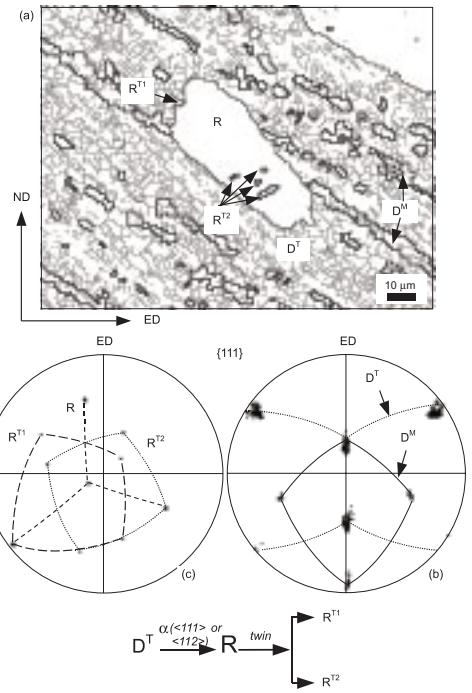

Fig. 14. The occurrence of the first generation of twins within an isolated grain. (a) part of the grain boundary map, and corresponding {111} pole figure from (b) the recrystallized grain and (c) the nearest as-deformed neighbourhood. Sample deformed 32%. SEM/EBSD measurements

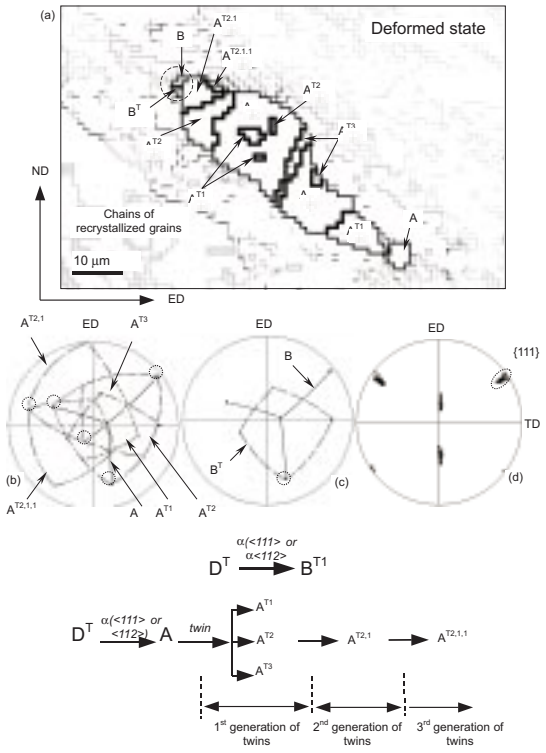

Fig. 15. Chains of new grains formed during the growth stage, showing two groups of nuclei with first recrystallization and then next generation twins. (a) 'grain boundary' map showing the microstructure, and the corresponding {111} pole figures containing orientations of (b) 'A' group of grains, (c) 'B' group of grains and (d) as-deformed state near the respective group of grains. SEM/EBSD measurements on a sample deformed 67%

The occurrence of the first recrystallization twins. Growth occurs by both boundary migration and twinning (from the initial nucleus orientation) on different {111} twinning planes followed by growth of the twinned areas. An example of the microstructure with the first generation of recrystallization twins (R^{T1} and R^{T2}) is shown in Fig. 14a. The large recrystallized area, denoted R, has a 25-28° <111> misorientation with respect to the neighbouring twinned areas of D^T. The misorientation axes are strongly linked with the pole of the co-directional slip plane. The {111} pole figures (Figs. 14b and c) show that one of the twinning variants within the recrystallized grain occurs on a {111} plane which is the same as that of the rotation axis.

The chains of primary nuclei with recrystallization twins. The role of the microstructure and microtexture after 67% deformation, on recrystallization will now be analysed in detail for the rather complicated case of groups of new grains with recrystallization twins. An example is presented on the 'grain boundary' map of Fig. 15a, showing two groups of grains (*A* and *B*) with recrystallization twins, forming compact chains of grains. The orientations of two groups of recrystallized grains, denoted as *A* and *B*, are presented in Figs. 15b and c. A detailed analysis of the as-deformed orientations near these grains (Figs. 15b) shows only one group of orientations near {110}<001> with relatively strong TD scattering due to shear banding, typical of this strain. The orientation relationship between the deformed, twinned matrix and the A and B grains again reveals the role, on the nucleation process of the near 25-40°(<111>–<112>) misorientations with respect to the D^T orientation group. The most complicated case of the A group of grains shows the first generation of recrystallization twins (on different twinning planes - A^{T1}, A^{T2}, and A^{T3}) and also the second ($A^{T2,1}$) and third generations of twins with orientation denoted as $A^{T2,1,1}$). The formation of the first and the subsequent generations of recrystallization twins considerably disturbs the primary orientation relationship between the grain with A orientation and the as-deformed components.

The above situation may be generalized as follows. For the most complicated cases of the chains of recrystallized grains *it is always possible to identify, within the set of orientations, the primary area, which possesses a near 25–40°(<111>–<112>) type misorientation, with respect to one of the two main groups of deformation components, D^M or more probably D^T*. But which of the different, possible recrystallization twinning systems will be successful during the growth appears too complicated to be explained.

4. Discussion

4.1. Crystal lattice changes as a result of the brass-type SB formation

In low SFE metals the formation of the fine T-M layer structure is the first step in the remarkable change of the overall texture. In accordance with previous studies [10–12, 20], {112}<111> oriented crystallites deformed in plane strain compression rotate first towards the so-called Dillamore orientation of {4 4 11}<11 11 8> and then undergo intense mechanical twinning [11]. The lattice rotations for the first-formed MSBs can be described as:

$$(112)[11\bar{1}]^{M} \rightarrow (4\ 4\ 11)[11\ 11\ \bar{8}]^{M}(7.9^{o}) - \textit{before twinning}$$

$$(4\ 4\ 11)[11\ 11\ \bar{8}]^{M} + (26\ 26\ 5)[\bar{5}\ \bar{5}\ 52]^{T} \rightarrow (114)[22\bar{1}]^{M} + (110)[001]^{T}(16^{o}) \rightarrow (118)[44\bar{2}]^{M}$$

$$+(17\ 17\ \bar{4})[4\ 4\ 34]^{T}(\sim 25^{o}) - \textit{after twinning as a result of SBs formation.}$$

The angles in parentheses indicate the angular rotation about the <110> axis with respect to the initial $C(112)[11\bar{1}]$ orientation. Mechanical twinning, in conjunction with dislocation slip on the CP slip systems ({111} planes parallel to the twinning plane) leads to a radical change of the initial sample shape. In channel-die compression the $\varepsilon_{TD/ED}$ shear is allowed, but the sample TD/ED plane is fixed by the compression plates. From the geometrical point of view, the successive stages of strain localization inside MSBs coincide with the appearance of lattice deflections inside restricted areas [2, 9, 12]. The unbalanced bending moments, resulting from the reactions of the anvils, are accommodated by local lattice kinking of the twinning plane with traces inclined at 40–42° to ED. The observed kink bands are a precursor to SB formation. As a result of this localized bending within narrow areas the crystal lattice and CP(111) slip (or twinning) planes are observed to change systematically. This brings the twinning planes inside the SB parallel to the shear plane. This position then facilitates further plastic strain by crystallographic slip in equally privileged co-planar slip systems lying on the re-oriented twinning plane.

The successive stages of this process are presented in Fig. 16. When the shear capacity is exhausted in the existing SB this implies SB nucleation in new bands. As

shown previously [9], the change of the sample height, as a result of strain localization inside the SB, depends on the band thickness and its inclination angle with respect to ED. These processes have been previously analysed in single crystals of Cu-2%wt Al [10, 11] and pure copper deformed at 77 K [8, 9, 12] as a result of rigid body rotation around the TD axis within narrow areas.

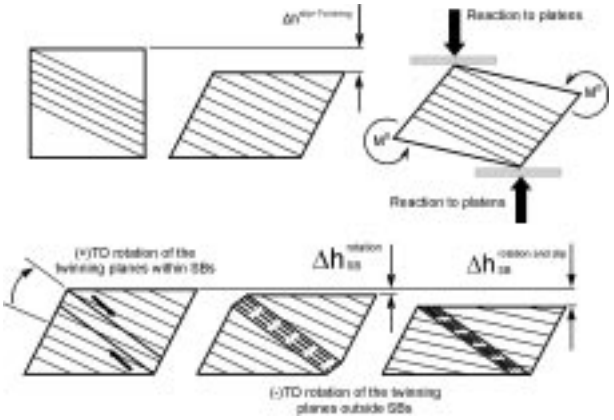

Fig. 16. Successive stages of the changes of the sample shape as a result of shear in the first family of MSB; twinning and shear along a particular SB leads to drastic changes of the crystal shape and strain accommodation on the sample scale

However, the mechanism of SB deformation is somewhat more complicated than this simple TD rotation. P a u l et al [12, 21, 22], based upon other systematic TEM local orientation measurements (orientation mapping), conclude that in addition to the TD rotation the orientations within the band are scattered by the rotations about one of the <112> poles. Because the rotation axes are always parallel to the most active slip planes, this confirms the hypothesis that for well-developed SBs one of the two (initially equivalent) co-planar slip systems plays a dominant role. Accordingly, rotation about one of the <112> poles must result from the operation of a single {111}<110>-type slip system. The angular proximity of the actual <112> rotation axis to one of the four <111> poles causes the relatively high stability of that particular pole compared to the other poles of the <111> family. Starting from D^M and D^T orientations (matrix and twins positions, respectively), the 65–70° <112>-type rotations ultimately lead, *via* Goss{110}<001> and twinned Goss G^T{114}<221>, to the Brass{110}<112> and S{123}<634> components [21–24]. This transformation can be described as follows:

$$D^M(4\ 4\ 11)[11\ 11\ \bar{8}]^M + D^T(26\ 26\ 5)[\bar{5}\ \bar{5}\ 52]^T \rightarrow$$
$$\rightarrow \text{ Brass}\{110\} < 112 > /\text{S}\{123\} < 634 >$$

In accordance with this model [12], it is also possible to explain the observed scattering of <111> poles, seen in Figs. 5b and 7f within SB areas, as a result of rotation around <112>-type axes. Consequently, both twinning on the CP slip plane and slip on the pairs of CP and co-directional (CD) systems together with unbalanced slip within a CP pair are responsible for the drastic texture changes, with their consequences on recrystallization nucleation.

4.2. Interpretation of the grain re-orientations during recrystallization

ON theory requires that the nuclei are part of the deformed structure. As expected, all observed cases of recrystallization begin in the zones with the highest stored energy (the MSB areas) and the first-formed nuclei possess orientations identified inside the MSB. As recrystallization proceeds, the successful new grains have well-defined crystallographic relations with the surrounding twinned matrix (OG model), in which growth occurs [25–32]. In all observed cases, areas of single, isolated nuclei (without recrystallization twins) possess a near 25-40°(<111>–<112>) orientation relationship with the as-deformed neighbourhood in the direction of highest growth rate. In this respect our results are qualitatively different from those obtained by other authors, in particular on non-twinning systems e.g. [16, 26–31], which show a predominance of near 40° <111> grain boundaries between deformed and recrystallized states.

N i e w c z a s et al [32] have recently shown that the recrystallization textures obtained from twinned material (copper deformed at 4.2 K) are composed of two sharp components, both of which were obtained by a 35-40° rotation about the twinning plane normal. This preferential growth produces new orientations derived from the two as-deformed components: twin and matrix. In general this is in accordance with the results presented here, in particular with regard to the influence of the two deformation components on the selection of the nuclei orientations. However, the 40° <111>-type OR introduces small complications into this interpretation. Namely, this kind of OR with respect to one as-deformed component implies the occurrence of another OR type with respect to the second one, and the conditions for 'consumption' of the T-M layers are significantly different. Privileged growth into both the twin and matrix layers requires a misorientation axis parallel to the twinning plane normal and a misorientation angle of 30°, as often observed in this study and in previous work by some of the present authors, e.g. [9, 10, 33]. From a crystallographic point of view, recrystallization growth in twinned structures is very similar to that observed in non-twinned metals of unstable orientations [33]. Also the different OR's between a new grain and the adjacent as-deformed areas are seen to be responsible for quite different growth rates [14, 34].

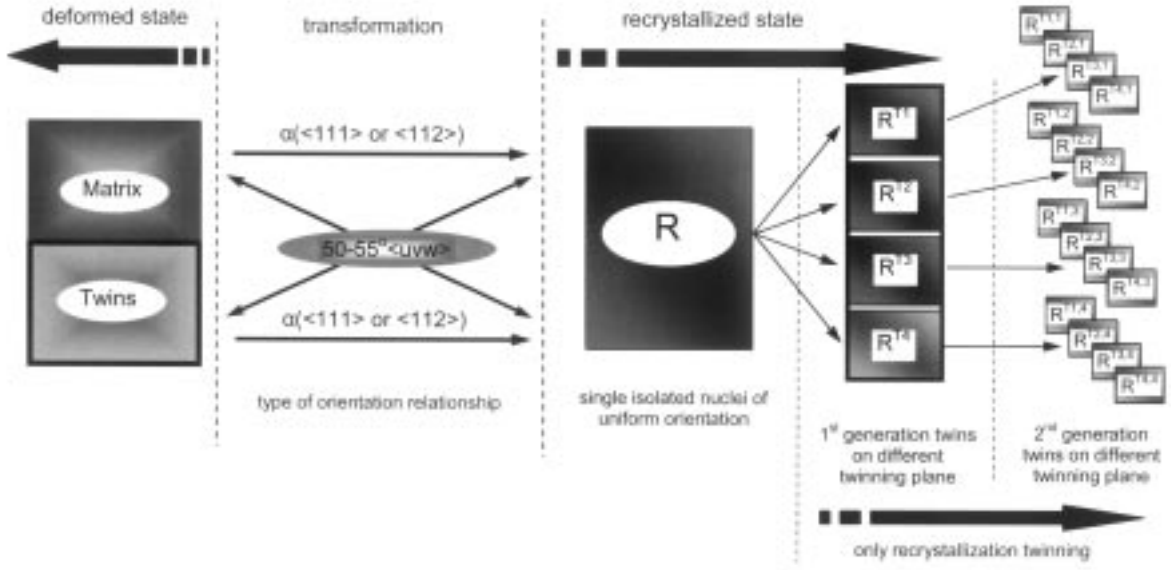

Fig. 17. Schematic representation of the orientation changes resulting from primary nucleation and successive recrystallization twinning observed at the early stages of recrystallization

The particular role of the orientations identified within the as-deformed SBs has been analysed previously in a more quantitative manner by examining the orientation distribution of the grains using SEM/EBSD measurements [9, 10, 14]. A quantitative analysis of the orientations of the first formed, recrystallized grains clearly shows that the presence of the SB microtexture components within the primary recrystallized grain microtextures is a direct result of an *increase of the intensities of particular poles as rotation axes*. This behaviour is also clearly observed in the present work (see Figs. 9b and c) and indicates the particular role, during recrystallization, of certain orientations situated at the limit of the range of the deformation microtexture. In the as-deformed state these SB orientations are only weakly visible on the 'global' deformation texture and are located at the limit of their spread. In the early stages of primary recrystallization, these <111> poles become gradually sharper. As recrystallization proceeds and 25–40°(<111> or <112>) rotations are developed in some areas of the bands, the intensity of the <111> pole of the most active {111} planes during deformation systematically increases. In this way for Goss-oriented areas the intensities of all four <111> poles of the dominant, as-deformed orientations increase at a new position characterised by an additional (+)TD rotation (i.e. the position of the main SB microtexture components). These observations, sometimes taken as confirmation of the ON model, are in fact due to the retention of particular <111> poles of the deformed state in new positions, only slightly deviated from the previous maxima by α(<111> or <112>) rotations, and which correspond to the recrystallized grains.

The results of the present study, together with those of earlier investigations [9, 10, 16, 35, 36] strongly suggest that invoking only one of the ON or OG mechanisms is inadequate for explaining the recrystallization textures. The fact that only a limited number of possible variants of new nuclei orientation are observed introduces a small modification of an old suggestion of Ibe & Lücke [37] and adopted by Duggan et al. [15, 17] into a combined ON/OG model (the so-called micro-growth selection). However, in our detailed investigations this classical misorientation described by OG model is replaced by a 25–40° rotation angle and rotation axes close to <111> or <112> directions.

The microtexture changes and mechanisms responsible for the transformations observed at the very early stages of recrystallization are schematically summarized in Figure 17. Independently of the nucleation site (matrix or twins) the most often observed OR is very close to the above 25-40° <111> or <112>. This type of misorientation with respect to one of the as-deformed components (twins or matrix) implies usually the existence of a second type of misorientation near 50-55° <uvw>, in accordance with the presence of the second, as-deformed component (excluding the situation when new grain orientations occur as a result of rotation around the twinning plane normal). The freshly formed grains then tend to grow by forming new grain boundaries through recrystallization twinning and hence radically change the orientation. The occurrence of different twinning vari-

ants (different twinning planes and several generations of recrystallization twins) then obscures the primary orientation relationship [38]. In this context recrystallization twinning can be regarded as a secondary mechanism (Fig. 17).

5. Summary and conclusions

The influence of SB deformation microstructure/microtexture on the early stages of recrystallization in deformed low SFE Ag has been characterised by local orientation measurements using a combination of TEM and SEM. It is shown that the dislocation slip mechanisms responsible for SB formation play a decisive role in these early recrystallization stages. Thus components of the internal SB microtexture are the starting point for the occurrence of new grain orientations. During deformation these bands provides the driving force for recrystallization.

As recovery proceeds and dislocations are removed from some areas the orientation changes to a frequently observed 25–40°(<111> or <112>)-type misorientation with respect to the adjacent deformation components. The presence of <112> directions as rotation axes in the process of primary nuclei formation (of uniform orientation) suggests a close link with the deformation process. The experiments show that the migration of newly formed grain boundaries and the 'consumption' of the as-deformed areas occurs by a mechanism linked to dislocation movement on the {111} planes. In particular, this is clearly visible within the SBs which accumulate high stored energy where nucleation occurs preferentially.

Once formed, the new grains exhibit a strong tendency to grow by forming new grain boundaries through recrystallization twinning and hence change their orientation. As recrystallization proceeds, the importance of twinning radically increases. However, this latter mechanism can be regarded only as a secondary mechanism which operates after the formation of the primary nuclei. Within the twinned structures of silver this automatically implies the formation of a second type of α<uvw> misorientation in accordance with the presence of the twin-matrix layers. In this way a limited set of new grain orientation variants may occur in this crystal at the very early stages of recrystallization.

In C-oriented silver single crystals, twinning also plays a decisive role in the formation of the cube-orientated grains. In accordance with the observed mechanism of nucleation the presence of the Brass-S components in the deformed state seems to be necessary for the formation of the near cube-oriented (<15°) nuclei by recrystallization twinning. In other words, a preferred set of orientations from the broad {122}<122> spectrum is necessary for exact cube grains occurrence.

REFERENCES

[1] B.J. Duggan, M. Hatherly, W.B. Hutchinson, P.T. Wakefield, Metal Sci **12**, 343 (1978).
[2] Y. Nakayama, K. Morii, Trans Japan Inst Met **23**, 422 (1982).
[3] K. Morii, H. Mecking, Y. Nakayama, Acta metall **33**, 379 (1985).
[4] J. Hirsch, K. Lücke, M. Hatherly, Acta metall **36**, 2905 (1988).
[5] J. Hirsch, K. Lücke, Acta metall **36**, 2863 (1988).
[6] G.D. Köhlhoff, A.S. Malin, K. Lücke, M. Hatherly, Acta metall **36**, 2841 (1988).
[7] J. Hirsch, J. Mat Sci Techn **6**, 1048 (1990).
[8] Z. Jasieński, H. Paul, A. Piątkowski, A. Litwora, J Mat Proc Techn **53**, 187 (1995).
[9] H. Paul, J.H. Driver, Z. Jasieński, Acta mater **50**, 815 (2002).
[10] H. Paul, J.H. Driver, C. Maurice, Z. Jasieński, Acta mater **50**, 4339 (2002).
[11] H. Paul, J.H. Driver, C. Maurice, Z. Jasieński, Mat Sci Engn **A359**, 178 (2003).
[12] H. Paul, A. Morawiec, E. Bouzy, J.J. Funderberger, A. Piątkowski, Metall Mater Trans 35A **35A**, 3775 (2004).
[13] L.E. Murr, Interfacial Phenomena in metals and alloys, Addison-Wesley, Reading MA; 376 (1975).
[14] A. Berger, P.J. Wilbrandt, F. Ernst, U. Klement, P. Haasen, Progress in Mater Sci **32**, 1 (1988).
[15] B.J. Duggan, M. Sindel, G.D. Köhlhoff, K. Lücke, Acta metall mater **38**, 103 (1990).
[16] J. Hjelen, R. Orsund, E. Nes, Acta metall mater **39**, 1377 (1991).
[17] B.J. Duggan, K. Lücke, G.D. Köhlhoff, C.S. Lee, Acta metall mater **41**, 1921 (1993).
[18] F.J. Humphreys, M. Hatherly, Recrystallization and related Annealing Phenomena. Oxford: Pergamon Press 1995.
[19] R.D. Doherty, D.A. Hughes, F.J. Humphreys, J.J. Jonas, D. Juul Jensen, M.E. Kassner, W.E. King, T.R. McNelly, H.J. McQueen, A.D. Rollet, Mat Sci Engn **A238**, 219 (1997).
[20] P. Wagner, O. Engler, K. Lücke, Acta Metall Mater **43**, 3799 (1995).
[21] H. Paul, J.H. Driver, C. Maurice, A. Piątkowski, Acta Materialia **55**, 575 (2007).
[22] H. Paul, A. Morawiec, E. Bouzy, J.J. Funderberger, A. Piątkowski, Microchimica Acta **147**, 181 (2004).
[23] H. Paul, J.H. Driver, C. Maurice, A. Piątkowski, Mat Sci Forum **467-470**, 177 (2004).

[24] H. Paul, J.H. Driver, Revue de Metallurgie **9**, 871 (2003).
[25] U. Klement, P. Haasen, Acta metall mater **41**, 1075 (1993).
[26] O. Engler, X.W. Kong, K. Lücke, Acta Mater **49**, 1701 (2001).
[27] A. Godfrey, D. Juul Jensen, N. Hansen, Acta Mater **49**, 2429 (2001).
[28] O. Engler, Acta mater **49**, 1237 (2001).
[29] S. Zaefferer, T. Baudin, R. Penelle, Acta mater **49**, 1105 (2001).
[30] I. Samajdar, R.D. Doherty, Scripta metall mater **32**, 845 (1995).
[31] A.A. Ridha, W.B. Hutchinson, Acta metall **30**, 1929 (1982).
[32] M. Niewczas, O. Engler, J.D. Embury, Acta Mater **52**, 539 (2004).
[33] J.H. Driver, H. Paul, J-C. Glez, C. Maurice, In: Hansen N., Huang X., Juul Jensen D., Lauridsen E.M., Leffers T., Pantleon W. editors. Proceedings of the 21st RISO International Symposium on Materials Science. Roskilde (Denmark); (2000), 35.
[34] O. Engler, Acta Mater **49**, 1237 (2002).
[35] H.J. Bunge, Texture analysis in materials Science. London: Butterworth 263 (1982).
[36] M. Blicharski, J. Liu, Hu. Hsun, Acta metall mater **43**, 3125 (1995).
[37] G. Ibe, K. Lücke. in: Margolin H, editor. Recrystallization, Grain Growth and Textures. Metals Park, Ohio: American Society for Metals 434 (1966).
[38] H. Paul, J.H. Driver, C. Maurice, A. Piątkowski, Acta Materialia **55**, 833 (2007).

Received: 5 February 2007.